# Effects of Ionic Strength on the Supramolecular Structure in Liquid Crystalline Solutions of Persistent Length DNA Fragments

**ARTICLE** *in* MACROMOLECULES · APRIL 1995

Impact Factor: 5.8 · DOI: 10.1021/ma00113a027 · Source: OAI



**5 AUTHORS**, INCLUDING:

Richard K Heenan
Science and Technology Facilities Council
**319** PUBLICATIONS **7,314** CITATIONS
SEE PROFILE

Wim Jesse
Leiden University
**22** PUBLICATIONS **452** CITATIONS
SEE PROFILE

Maxim E Kuil
Leiden University
**42** PUBLICATIONS **692** CITATIONS
SEE PROFILE

Johan R C van der Maarel
**108** PUBLICATIONS **1,717** CITATIONS
SEE PROFILE

# Effects of Ionic Strength on the Supramolecular Structure in Liquid Crystalline Solutions of Persistent Length DNA Fragments

**K. Kassapidou,† R. K. Heenan,‡ W. Jesse,† M. E. Kuil,† and J. R. C. van der Maarel*,†**

*Department of Physical and Macromolecular Chemistry, Gorlaeus Laboratories, Leiden University, P.O. Box 9502, 2300 RA Leiden, The Netherlands, and Rutherford Appleton Laboratory, ISIS Facility, Chilton, Didcot, Oxon OX11 0QX, England*

*Received December 13, 1994; Revised Manuscript Received February 14, 1995*®

ABSTRACT: Cholesteric liquid crystals of persistence length DNA fragments (contour length 55 nm) were studied with small angle neutron scattering. The cholesteric axis was oriented either perpendicular or parallel to the incoming neutron beam with the help of a magnetic field in the range 0.8−1.65 T. A single diffraction peak is observed, which shows in the perpendicular configuration an angular anisotropy in intensity. A moderate magnetic field strength dependence of the anisotropy has been observed, but at the higher field strength the liquid crystal is nearly completely aligned. A decrease in peak intensity as well as anisotropy is observed with increasing ionic strength, but fixed DNA concentration. This indicates a decrease in position and orientation order with increased screening of electrostatic interactions. From a comparison of the anisotropic data to the scattering contribution of a single fragment, the standard deviation of the presumed Gaussian orientation distribution could be derived. The results compare favorably with the second virial theory of lyotropic liquid crystals, provided that electrostatic interactions in terms of an ionic strength dependent effective diameter and DNA flexibility are taken into account.

## Introduction

Liquid crystalline mesophases of DNA can be found *in vivo*: plasmid DNA in bacteria, viruses, and mitochondria.[1−3] The condensed forms provide a means to store the genetic material in a relatively small volume. The ability of DNA to form a cholesteric liquid crystal has initially been observed *in vitro* by Robinson in 1961.[4] Persistence length DNA fragments (with an approximate length of 50 nm) show a series of phase transitions from the isotropic phase, via the cholesteric phase, eventually to a hexagonal structure.[5,6] These DNA fragments can be considered as flexible highly charged rods, each surrounded by a double layer formed by counterions and possibly added low molecular weight salt. The critical concentration for the isotropic to cholesteric phase transition depends on DNA molecular weight, temperature, and ionic strength.[7]

In the cholesteric phase, the director representing the local average DNA fragment orientation is perpendicular and rotates about the cholesteric axis with a pitch of the order 2 $\mu$m.[8] The pitch is essentially independent of supporting electrolyte concentration and is much larger than the characteristic intermolecular distances.[7] On a molecular distance scale, the liquid crystal can be considered nematic. The nucleotides possess a negative anisotropic diamagnetic susceptibility, and DNA fragments tend to arrange with their long axes perpendicular to the direction of an external magnetic field.[9−11] In the liquid crystal, this results in an alignment of the cholesteric axis along the field.[8] When the director is normal to the field at all points, no magnetic distortion energy is required and the pitch is independent of field strength.[12]

In previous work, the cholesteric liquid crystalline phase has been investigated by small angle neutron scattering.[13] These experiments were done with samples without added low molecular weight salt and at three different DNA concentrations. The cholesteric axis was aligned either parallel or perpendicular to the incoming neutron beam with a magnetic field (see Figure 1). The scattered intensity is proportional to the Fourier transform of the DNA density correlation function. In the perpendicular configuration anisotropic scattering is observed. From a comparison of the anisotropic intensities to the scattering contribution of a single fragment (form function), information on the orientation ordering could be derived. The orientation distribution is assumed to be Gaussian and the standard deviation was found to be approximately 20°. The standard deviation refers to a distribution in cholesteric axis orientation and/or fragment orientation with respect to the cholesteric axis.

The previous experiments were performed using a magnetic field strength 0.8 T in the direction perpendicular to the incoming neutron beam. However, the 0.8 T field might not have been sufficiently intense to induce full alignment of the cholesteric axis. For instance, magnetic-field-induced birefringence experiments on nematic droplets of tobacco mosaic virus particles (TMV) show that the principle effect of the magnetic field is to align them along the field, which occurs in the range 1−2 T.[14] In the present contribution, the distribution in cholesteric axis orientation has been further investigated by performing neutron-scattering experiments with various magnetic field strengths in the range 0.8−1.65 T.

DNA is a polyelectrolyte and the extent to which electrostatic interactions are screened is expected to be related to the solution ionic strength. In the theory of charged polyions an effective diameter is introduced, which decreases with increasing ionic strength.[15−17] The main purpose of the present contribution is to investigate the effects of electrostatic screening on the liquid crystalline orientation and position order. To this end, neutron-scattering experiments are performed at a fixed

* To whom correspondence should be addressed.
† Leiden University.
‡ Rutherford Appleton Laboratory.
® Abstract published in *Advance ACS Abstracts,* April 1, 1995.

0024-9297/95/2228-3230$09.00/0 

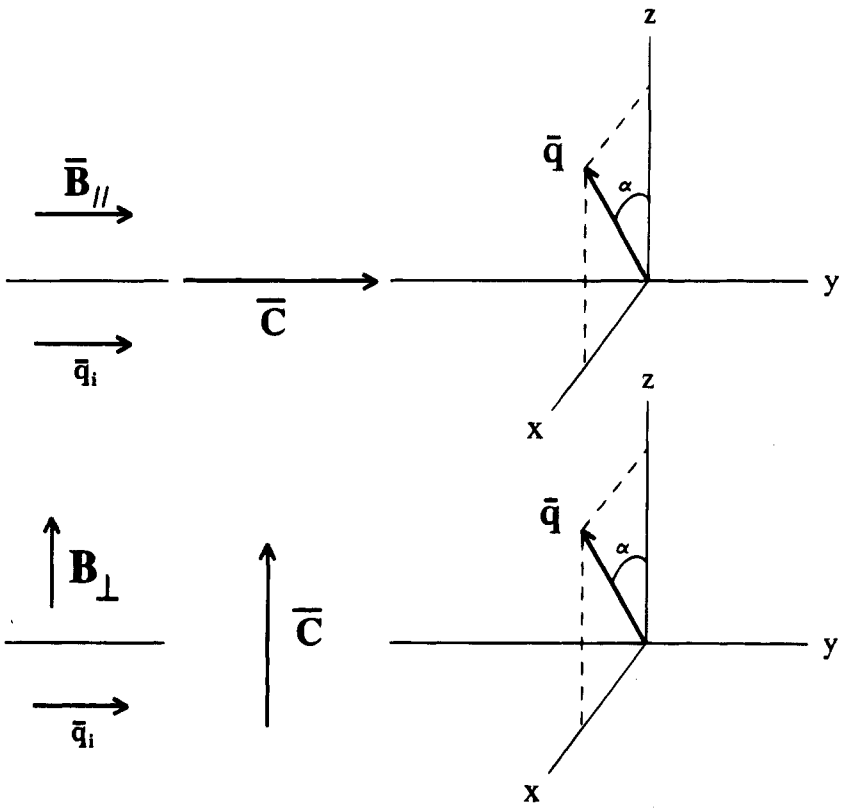


**Figure 1.** Definition of the experimental setup and sample geometry. The vectors $B_{||}$ and $B_\perp$ denote the direction of the magnetic field in the parallel (top) and perpendicular (bottom) configuration, respectively. The direction of the incoming beam is indicated by $\mathbf{q}_i$, and $\mathbf{q}$ denotes the momentum transfer. The two-dimensional detector is in the $xz$-plane with its horizontal along the $z$-axis. The average orientation of the molecules (director) is perpendicular to and rotates about the cholesteric axis $\mathbf{C}$ with a pitch of the order $10^{-6}$ m.

DNA concentration in different solvents with various amounts of NaCl or $MgCl_2$ (the previous samples were prepared without added low molecular weight salt). In a sufficiently strong magnetic field, the distribution in cholesteric axis orientation is saturated and the derived values of the standard deviation refer to the distribution of the DNA fragments with respect to the cholesteric axis.

The standard deviations and its ionic strength dependence will be compared to a theory for lyotropic nematic liquid crystals of rodlike or persistent polymer chains. In Onsager's original treatment, the phase behavior and orientation order are analyzed on the basis of interactions between two thin hard rods represented by the second virial coefficient in the free energy expansion.[18] It was shown by Khokhlov, Semenov,[19] and Odijk[20] that chain flexibility has a substantial influence on the orientation entropy. The effects of electrostatic interactions between polyelectrolyte rigid rods were included in the Debye–Hückel approximation by Stroobants et al.[17]

The second virial theory accounts for a substantial body of experimental data on uncharged persistent polymers, although the fitted values of the persistent length are generally larger than those obtained by independent measurements.[21] For the TMV polyelectrolyte, Caspar and co-workers measured the coexistence concentrations and orientation distribution with magnetic-field-induced birefringence and X-ray scattering, respectively.[14,22,23] The results compare well with the values predicted by Onsager's theory, indicating the insignificance of the virus particle flexibility. For persistent length DNA fragments, it will be shown that it is mandatory to include both electrostatic interactions in terms of an effective diameter and polyion flexibility in the second virial theory.

## Theory

In the present DNA solutions the nucleotide scattering length contrasts exceeds the corresponding values of the small ions by 2 orders of magnitude. Accordingly, the scattering is dominated by the DNA structure. The coherent part of the solvent-subtracted scattered intensity reads[13]

$$I(\mathbf{q}) = c\bar{b}_m^2 S_{mm}(\mathbf{q}) \tag{1}$$

with $c$ the concentration in number of nucleotides per unit volume and $\mathbf{q}$ the momentum transfer vector. The nucleotide monomer structure function is denoted by $S_{mm}(\mathbf{q})$. The nucleotide contrast parameter $\bar{b}_m$ has been calculated according to the calf-thymus DNA base composition A:G:C:T:5-methyl-cytosine = 0.28:0.22:0.21:0.28:0.01[24] and the scattering lengths reported by Jacrot.[25] In pure water, this scattering length contrast takes the value $11.38 \times 10^{-12}$ cm.

The DNA structure function is the spatial Fourier transform of the nucleotide density correlation function

$$S_{mm}(\mathbf{q}) = \frac{1}{\varrho_m V}\int_V d\mathbf{r}\, e^{i\mathbf{q}\mathbf{r}}\langle \varrho_m(0)\varrho_m(\mathbf{r})\rangle \tag{2}$$

Under neglect of correlation between intermolecular interactions and molecular conformation, the structure function can be expressed as a sum of the form function

$F(\mathbf{q})$ and the intermolecular interference contribution $S^{inter}(\mathbf{q})$:

$$S_{mm}(\mathbf{q}) = F(\mathbf{q}) + S^{inter}(\mathbf{q}) \quad (3)$$

The form function represents the scattering of a single DNA fragment and is a monotonic decreasing function with $|\mathbf{q}|$. The contribution $S^{inter}(\mathbf{q})$ induces a maximum in the scattered intensity at a momentum transfer $|\mathbf{q}_m|$. For sufficiently high values of momentum transfer beyond the maximum, the intermolecular interference contribution becomes progressively less important. In the absence or neglect of intermolecular interference, the structure function reduces to the DNA form function.

The DNA fragment form function is approximated by the form function of a uniform rod with radius $r_p$ and length $L$. For a certain orientation of the DNA fragment with respect to the momentum transfer vector $\mathbf{q}$, the form function reads[13]

$$F(q,\mu) = N_m\left[\frac{\sin(q\mu L/2)2J_1(qr_p\sqrt{1-\mu^2})}{(q\mu L/2)qr_p\sqrt{1-\mu^2}}\right]^2 \quad (4)$$

with $q = |\mathbf{q}|$ and $N_m$ is the number of nucleotides per fragment. $J_1$ is the first-order Bessel function of the first kind. The fragment orientation is given by the inproduct $\mu = \mathbf{p}\cdot\mathbf{q}$, $\mathbf{p}$ being the unit vector of the DNA helix long axis. An orientation average of the form function has to be performed, taking into account the magnetic-field-induced orientation alignment. For a detailed description of the definitions of the various vectors and axes the reader is referred to ref 13.

In the perpendicular configuration, the magnetic field is applied along the horizontal of the detector. The cholesteric axis is aligned along the field with a certain distribution in orientation. The form function is evaluated by using a DNA fragment orientation probability function $P(\theta,\varphi)$. The projected angle within the plane perpendicular to the magnetic field is denoted by $\varphi$, whereas the angle $(\theta - \pi/2)$ gives the tilt away from this plane. The distribution in $\varphi$ is isotropic due to the helical distribution in director orientation about the cholesteric axis. The distribution in angle $\theta$ is assumed to be Gaussian and peaked around $\theta = \pi/2$

$$P(\theta,\varphi) = \frac{1}{2\pi}P(\theta) = \frac{1}{2\pi}\exp\left(-\left(\theta - \frac{\pi}{2}\right)^2/2\sigma^2\right) \quad (5)$$

with $\sigma$ the standard deviation. The standard deviation $\sigma$ refers to a distribution in cholesteric axis orientation and/or a distribution in tilt angle of an individual DNA fragment with respect to the cholesteric axis. With distribution eq 5, the orientation-averaged form function takes the form[13]

$$F(\mathbf{q}) = F(q,\alpha) = \frac{1}{2\pi}\int_0^{2\pi}d\varphi \int_0^{\pi}d\theta \sin(\theta)\, P(\theta)\, F(q,\mu)/\int_0^{\pi}d\theta \sin(\theta)\, P(\theta) \quad (6)$$

with $\alpha$ being the angle between the momentum vector $\mathbf{q}$ and the horizontal of the detector. The integrations have to be numerically performed.

In the parallel configuration the magnetic field is perpendicular to the detector and, hence, to the $\mathbf{q}$ vector for any value of $\alpha$. This is exactly the same situation as in the perpendicular configuration with $\alpha = \pi/2$. Accordingly, the corresponding isotropic form function follows immediately from eq 6 with $\alpha = \pi/2$.

For sufficiently intense magnetic field strengths, the cholesteric axis is perfectly aligned along the field. In this situation, $\sigma$ describes the distribution in tilt angle away from the plane perpendicular to the cholesteric axis. The cholesteric pitch is approximately 2 $\mu$m,[7,8] and hence, the DNA fragment system can be considered locally nematic. The values of $\sigma$ can be interpreted in terms of a theory for lyotropic rodlike liquid crystals based on the second virial approximation. This theory is originally due to Onsager[18] and extended by Stroobants et al. to include electrostatic interactions.[17] Theoretical work by Khokhlov and Semenov shows the importance of semiflexibility effects on the order parameter and phase diagram.[19] For a review on the theory of lyotropic polymer liquid crystals the reader is referred to the paper by Odijk.[20]

In the Debye–Hückel approximation, for two rodlike polyelectrolytes skewed at an angle $\phi$ the electrostatic potential has the form[15,16]

$$\frac{w}{kT} = \frac{Ae^{-\kappa x}}{\sin\phi} \quad (7)$$

where $x$ denotes the shortest distance between the central axes and the constant $A$ depends on the polyion properties. For a discussion of the latter parameter the reader is referred to ref 17. For solutions in excess simple salt with ionic strength $I$, the screening length $\kappa^{-1}$ is given by $\kappa^2 = 8\pi QI$ with the Bjerrum length $Q = e^2/\epsilon kT$.

In the second virial approximation, the Helmholtz free energy of an anisotropic solution of $N$ rodlike polyelectrolytes reads[17]

$$\frac{\Delta F}{NkT} = \text{constant} + \ln c_p + \sigma_E + b^{eff}c_p(\varrho + h\eta) \quad (8)$$

with $\sigma_E$ the orientation entropy, $b^{eff}$ the second virial coefficient, and $c_p$ the rod number concentration $N/V$. The parameters $\varrho$ and $\eta$ depend on the orientation distribution of the rods and will be discussed below. For rods with length $L$ and bare diameter $D$, the second virial coefficient is proportional to the effective excluded volume and takes the form

$$b^{eff} = \frac{\pi}{4}L^2D^{eff}\left(1 + \frac{4D^{eff}}{L}\right) \quad (9)$$

with effective diameter

$$D^{eff} = D + \kappa^{-1}(\ln A' + \gamma + \ln 2 - {}^1/_2) \quad (10)$$

Here, $\gamma$ denotes Euler's constant and $A' = Ae^{-\kappa D}$. The second virial coefficient includes end effects according to ref 26. The parameter $h$ is the ratio of the Debye length and the effective diameter: $h = \kappa^{-1}/D^{eff}$.

The parameters $\varrho$ and $\eta$ are proportional to the orientational pair excluded volume:

$$\varrho = \frac{4}{\pi}\langle\langle\sin\phi\rangle\rangle_a \quad (11)$$

$$\eta = \frac{4}{\pi}\langle\langle-\sin\phi\ln(\sin\phi)\rangle\rangle_a - (\ln 2 - {}^1/_2)\varrho \quad (12)$$

where the brackets $\langle\langle\ldots\rangle\rangle_a$ denote the orientation average of the two rods in the anisotropic phase. To evaluate $\varrho$ and $\eta$, an orientation distribution function has to be

chosen. With Onsager's original distribution function[18]

$$P(\theta) = \frac{\alpha_D \cosh(\alpha_D \cos(\theta - \pi/2))}{4\pi \sinh \alpha_D} \quad (13)$$

these parameters take the form[17]

$$\varrho(\alpha_D) = 4(\pi\alpha_D)^{-1/2}\left[1 - \frac{15}{16\alpha_D} + ...\right] \quad (14)$$

$$\eta(\alpha_D) = 2(\pi\alpha_D)^{-1/2}\left[(\ln \alpha_D - 2 \ln 2 - 1 + \gamma) \times \left(1 - \frac{15}{16\alpha_D} + ...\right) + \frac{5}{2\alpha_D} + ...\right] \quad (15)$$

These expansions converge rapidly for sufficiently large values of the distribution width parameter $\alpha_D$, and hence, only the terms up to $\alpha_D^{-1}$ are retained. For a highly ordered state with $\alpha_D \gg 1$, Onsager's trial function eq 13 takes the Gaussian limit eq 5 (apart from an arbitrary normalization constant) and $\alpha_D = \sigma^{-2}$. For the present experimental values of the standard deviation, both distribution functions are equal within e.g., 2%, with the main difference in the flanks. Accordingly, the expansions eqs 14 and 15 will be used in the expression of the free energy eq 8, together with the Gaussian approximation of the orientation entropy $\sigma_E$.

In the present contribution two different expressions of the orientation entropy $\sigma_E$ will be verified. Both expressions are strictly valid in the Gaussian approximation of the orientation distribution function. For rigid rods without any flexibility, one has[20]

$$\sigma_E = \ln \alpha_D - 1 \quad (16)$$

As will be shown below, this expression yields too low values of the standard deviation $\sigma$. It appears to be necessary to take flexibility effects into account. For semiflexible polymers, Odijk has derived an approximate equation for the orientation entropy[20]

$$\sigma_E = \ln \alpha_D + \frac{1}{6}\alpha_D N_p + \frac{5}{12}\ln\left(\cosh\left(\frac{1}{5}\alpha_D N_p\right)\right) - \frac{19}{12}\ln 2 \quad (17)$$

Here, $\sigma_E$ has an explicit contour length dependence expressed as the number $N_p$ of persistence length units. For the present DNA fragments $N_p$ is of order unity.

The standard deviation $\sigma$ ($=\alpha_D^{-1/2}$) can be obtained by minimization of the free energy eq 8, together with the expressions for $\varrho$, $\eta$, and $\sigma_E$ (by solving $\partial\Delta F/\partial\sigma = 0$). Generally, two roots for $\sigma$ are obtained; the higher value has no physical meaning. The input parameters are the product of the second virial coefficient and the polymer number concentration, $b^{eff}c_p$, and the twist parameter $h$. For rigid rods with $\varrho(\alpha_D) = 4(\pi\alpha_D)^{-1/2}$, $\sigma_E = \ln \alpha_D - 1$, and neglect of the twist parameter ($h = 0$), one obtains[20]

$$\sigma = \alpha_D^{-1/2} = \pi^{1/2}/2(b^{eff}c_p)^{-1} \quad (18)$$

The standard deviation is inversely proportional to $b^{eff}c_p$. For higher order approximations of $\varrho$, nonzero values of $h$, and flexibility effects, the minimization procedure has to be executed by a numerical method.

## Experimental Section

Persistence length DNA fragments were obtained by a micrococcal nuclease digestion of calf thymus chromatin, following the procedure described before.[13,27] The molecular weight distribution was determined by gel permeation chromatography with light-scattering detection.[28] Some low ((1–6) × $10^4$) as well as some high (≈2 × $10^5$) molecular weight DNA was detected. Seventy-five percent of the material had a molecular weight of 1.08 × $10^5$, with $M_w/M_n$ < 1.1 (163 base pairs). The ratio of the specific UV absorbance, $A_{260}/A_{280}$ was 1.87, indicating that the material was essentially free of protein.[29] The sodium content was verified by atomic absorption spectrometry. This showed that the counterions were exclusively sodium and confirmed the absence of simple salt. The hypochromic effect at 260 nm was more than 30%, indicating that the DNA was in the native double helix form.

**Table 1. NaDNA Concentration and Solvent Composition of the Various Samples**

| sample | solvent | $c$ (nucleotide/nm$^3$) |
|---|---|---|
| G1 | $H_2O$ | 0.36 |
| G2 | $H_2O$ | 0.44 |
| G3 | $H_2O$ | 0.52 |
| I | $H_2O$ | 0.45 |
| II | 0.25 M NaCl | 0.46 |
| III | 0.75 M NaCl | 0.46 |
| IV | 1.51 M NaCl | 0.46 |
| V | 0.08 M $MgCl_2$ | 0.46 |

Five samples were prepared by dissolving NaDNA in five different solvents. The solvents are pure water, NaCl and $MgCl_2$ solutions. The simple electrolytes are of analytic quality from Merck (Darmstadt). The DNA and simple salt concentrations are collected in Table 1. All concentrations are determined by weight, using the water content in the freeze-dried material and the NaDNA partial molar volume 165 cm$^3$/mol. The NaDNA concentration is expressed as number of nucleotides per cubic nanometer. It should be noted that sample IV contains a mixed cation, i.e. sodium originating from dissolved DNA material and added $Mg^{2+}$.

The samples were fully liquid crystalline as no phase separation was observed by visual inspection with crossed polarizers. A droplet of each solution was deposited between a slide and coverslip in order to be examined with a Zeiss Axiolab polarization microscope. The observed characteristic fingerprint textures confirmed the cholesteric structure.

Neutron-scattering experiments were performed at the LOQ small angle scattering instrument, situated on the pulsed spallation neutron source of the ISIS facility, Rutherford Appleton Laboratory, Didcot, U.K. The incident wavelength is 2–10 Å at a pulse rate of 25 Hz. The scattered radiation was detected using an effective 64 cm diameter two-dimensional detector (64 × 64 pixels). The detector was placed at a distance of 4.4 m from the sample position, allowing a momentum transfer range of 0.006–0.2 Å$^{-1}$. The wavelength of each neutron arriving at the detector was calculated with the time of flight method.[30] Quartz cells with 1 mm path length were used. The temperature was kept at 298 K with the use of a water thermostat.

Two sets of experiments were performed, with a magnetic field subsequently applied perpendicular and parallel to the incoming neutron beam. In the perpendicular configuration, sample I was measured using field strengths of 0.8, 1.5, and 1.65 T. The other samples were measured with the highest attainable field strength of 1.65 T only. In the parallel configuration, the highest attainable intensity of the magnetic field was 1.3 T. Sample II was measured in the perpendicular configuration only.

The counting time per sample was approximately 4 h. The scattering was normalized allowing for the wavelength dependent sample transmission, incident beam monitor, and detector efficiency. Absolute scattered intensities were scaled by reference to the coherent scattering from a partially deuterated polystyrene sample. The scattering of pure water was subtracted and no additional incoherent scattering correction was performed. It was observed that the reference solvents (i.e. the saline solutions without DNA) do not show significant scattering in the present range of momentum transfer.

## Results and Discussion

**Two-Dimensional Scattering Patterns.** Small angle neutron scattering experiments were done with a magnetic field subsequently applied perpendicular and parallel to the incoming neutron beam (see Figure 1). These two different configurations are indicated by $B_\perp$ and $B_\parallel$, respectively. The scattering patterns (data not shown) show the same qualitative features as the previously reported results without excess simple salt.[13] For both configurations, the two-dimensional scattering patterns show a circular maximum. In the $B_\parallel$ configuration isotropic scattering is observed, whereas for $B_\perp$ the intensity is anisotropic. These characteristic scattering patterns originate from the cholesteric liquid crystalline structure. Due to the negative anisotropic diamagnetic susceptibility of the nucleotides, DNA tends to arrange with its long axis perpendicular to the direction of a magnetic field.[8-11,31] In the cholesteric phase, this results in an alignment of the cholesteric axis along the field. The average direction of the DNA fragments is denoted by the director, which rotates about the cholesteric axis. In the fingerprint polarization microscopy textures, the helical pitch varies from $1.5 \times 10^{-6}$ to $2.3 \times 10^{-6}$ m with an average value of $2.0 \times 10^{-6}$ m. No significant effect of the ionic strength was observed, in accordance with the results of Rill et al.[7] In the $B_\parallel$ configuration the cholesteric axis is perpendicular to the two-dimensional detector. The intensity is isotropic due to the helical distribution of the director parallel to the detector. For the other configuration the cholesteric axis is parallel to the detector. Here, anisotropic scattering is observed, because the orientation of the cholesteric axis with respect to the momentum transfer vector varies with the direction of momentum transfer.

As discussed in the theoretical section, the data represent a sum of the monotonously decreasing form function and an unknown intermolecular solution structure function. The latter contribution becomes progressively more negative for smaller values of momentum transfer and, hence, a maximum is observed. The corresponding momentum transfer is denoted by $\mathbf{q}_m$. The maximum owes its existence to intermolecular interference effects and indicates the distance scale over which these interferences are important. For both configurations a circular maximum is observed, i.e. $|\mathbf{q}_m|$ is insensitive to the orientation of the cholesteric axis with respect to the direction of momentum transfer. This shows that any difference in characteristic intermolecular structure perpendicular and parallel to the cholesteric axis is beyond observation. Two-dimensional detector averages can be performed, since the diffraction patterns are circular. An angular detector segment resolved analysis will subsequently be discussed.

**Angular Averaged Intensities.** Figures 2–4 display the angular averaged intensities divided by the constant $c\bar{b}_m^2$ versus the momentum transfer $|\mathbf{q}|$. The data represent the partial DNA structure function $S_{mm}$, if the scattering due to small ions and the incoherent scattering can be neglected. Figures 2 and 3 illustrate the effects of added simple salt on the scattering in the parallel ($B_\parallel$ = 1.3 T) and perpendicular ($B_\perp$ = 1.65 T) configurations, respectively. Figure 4 displays the angular averaged intensity of sample I (without added salt) for three different magnetic field strengths in the perpendicular direction ($B_\perp$ = 0.8, 1.5, and 1.65 T). The signal of the latter sample is the most intense and, therefore, is the most sensitive to magnetic field strength effects.

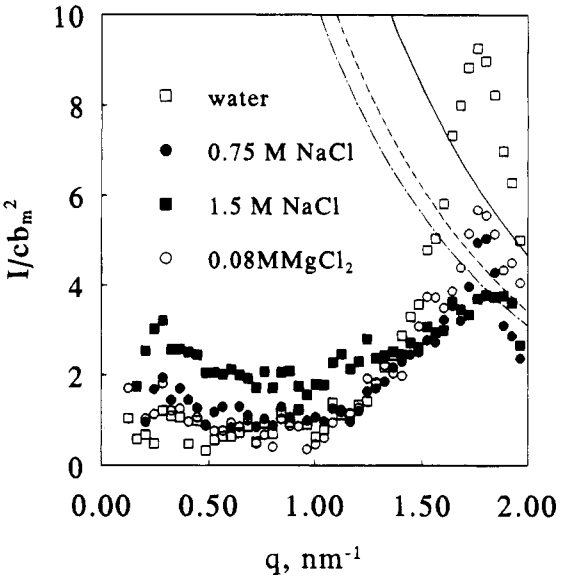


**Figure 2.** Angular-averaged scattered intensities divided by the constant $c\bar{b}_m^2$ versus momentum transfer in the parallel configuration ($B_\parallel$ = 1.3 T). The solvents are indicated in the figure. The solid line represents the isotropic orientation average of the form function of a uniform rod with length $L$ = 55 nm and radius $r_p$ = 0.8 nm. The dotted-dashed and dashed lines show the average with $\alpha = \pi/2$ and $\sigma$ = 15 and 30°, respectively.

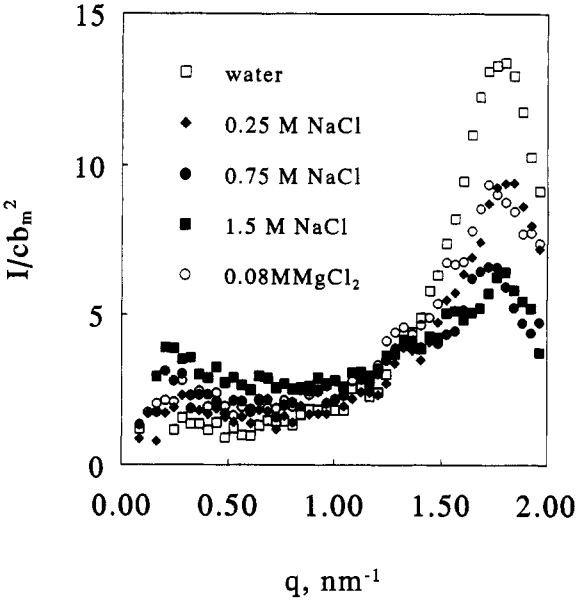


**Figure 3.** As in Figure 2, but in the perpendicular configuration ($B_\perp$ = 1.65 T).

The results displayed in Figure 2 are qualitatively similar to the results in Figure 3. Quantitatively, in the perpendicular configuration the intensities are roughly a factor 1.5 more intense compared to those in the parallel configuration. This effect cannot be explained by a difference in employed magnetic field strength. As shown by Figure 4, a decrease of the magnetic field strength from 1.65 to 0.8 T results in a 15% decrease in intensity. This could only be checked in the perpendicular configuration, since in the parallel configuration the highest attainable magnetic field strength was 1.3 T. The difference in intensity between both configurations is due to a different orientation of the cholesteric axis with respect to the detector. In the

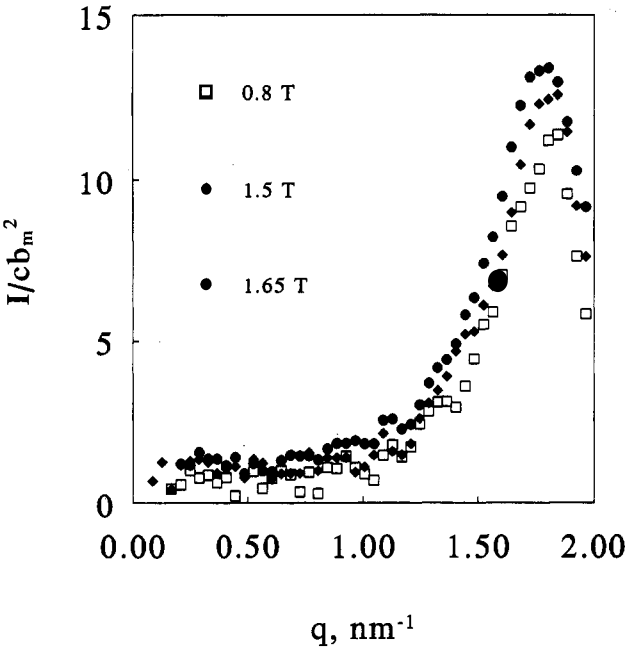


**Figure 4.** Angular-averaged scattered intensities divided by the constant $cb_m^2$ for DNA in water without added simple salt (sample I). The magnetic field is in the perpendicular direction with strengths as indicated in the figure.

perpendicular configuration, the magnetic field strength dependence of the intensity (Figure 3) is probably related to a distribution in cholesteric axis orientation. These features will be detailed below when angular segment resolved intensities are presented. Now, the added salt dependence of the two-dimensional detector averaged results will be discussed.

As was discussed before, the value of $|\mathbf{q}_m|$ is insensitive to the direction of momentum transfer. This is confirmed by Figures 2 and 3, for both configurations the maximum shows up at the same value of $|\mathbf{q}| \approx 1.8$ nm$^{-1}$. Furthermore, the position of the maximum is insensitive to the presence of added simple salt. As was discussed in previous work, $|\mathbf{q}_m|$ is inversely related to intermolecular distances or proportional to $c^{1/2}$, with $c$ being the DNA concentration.[13,32] For most of our samples the concentrations are equal, and hence, the data show the same $|\mathbf{q}_m|$. For sample II there is a small shift to higher $|q|$ values, related to a slightly higher DNA concentration. The presence of added simple salt has no influence on the average intermolecular distance. This result differs from SAXS observations by Wang and Bloomfield on more diluted isotropic solutions of similar DNA fragments (72 mg/mL).[32] They found that $|\mathbf{q}_m|$ is initially insensitive to salt concentration until about 0.1 M NaCl, at which value it decreases dramatically. This behavior was attributed to a transition from random to more or less parallel arrangement of the DNA fragments as the salt concentration decreases. Another explanation may be the onset of salt-induced aggregation[33] or blue phase structures.[34] In the present situation, the liquid crystalline orientation order is preserved, although the distribution width depends on salt concentration (see below).

DNA is a polyelectrolyte and the electrostatic interactions are expected to be related to the solution ionic strength. The ionic strength has been calculated according to $I = {}^1/_2\Sigma c_i z_i^2$, with $c_i$ the small ion concentrations. The results are collected in Table 2. In these concentrated samples, the contribution of counterion originating from DNA cannot be neglected. An uncondensed counterion fraction 0.24 has been taken into account in the calculation.[35,36] For the solution in 0.08 M $MgCl_2$, this procedure presents some difficulties due to possible condensation of divalent $Mg^{2+}$. This effect has been neglected and the corresponding entry in Table 2 should be interpreted as an approximate value. The ionic strengths of the solutions in 0.25 M NaCl and 0.08 M $MgCl_2$ are of the same order of magnitude. As displayed in Figures 2 and 3, the structure functions of both samples are similar. Apparently, the structure is determined by ionic strength, any possible specific effects related to divalent $Mg^{2+}$ are beyond observation.

**Table 2. Ionic Strength $I$, Effective DNA Diameter $D^{eff}$, the Parameter $h$, Magnetic Field Strength $B_\perp$, and Distribution Width $\sigma$[a]**

| sample | $I$ (mol/L) | $D^{eff}$ (nm) | $h$ | $B_\perp$ (T) | $\sigma$ (deg) |
|---|---|---|---|---|---|
| G1[b] | 0.07 | 6.9 | 0.17 | 0.8 | 20 |
| G2[b] | 0.09 | 6.3 | 0.17 | 0.8 | 21 |
| G3[b] | 0.10 | 5.9 | 0.16 | 0.8 | 18 |
| | | | | 0.8 | 20 |
| I | 0.09 | 6.3 | 0.16 | 1.5 | 15 |
| | | | | 1.65 | 15 |
| II | 0.35 | 4.0 | 0.13 | 1.65 | 20 |
| III | 0.85 | 3.2 | 0.10 | 1.65 | 25 |
| IV | 1.60 | 2.9 | 0.08 | 1.65 | 30 |
| V | 0.34[c] | 4.1 | 0.13 | 1.65 | 20 |

[a] The effective diameter has been calculated with a bare diameter $D = 2.4$ nm. [b] Data from ref 13. [c] Condensation of $Mg^{2+}$ has been neglected.

With increasing ionic strength, the intensity at the peak position decreases with a concurrent increase of the scattering at small values of momentum transfer. The latter behavior is characteristic for polyelectrolyte solutions with excess salt and is related to an increase in osmotic compressibility.[37] The decrease in peak intensity is due to a change in positional and orientational order. To estimate these effects, the structure functions are compared to the molecular form function representing the DNA fragment and taking into account the liquid crystalline orientation order.

In previous work it was shown that at and beyond the peak maximum the structure function more or less represents the molecular form function of a uniform rod with length $L = 55$ nm and radius $r_p = 0.8$ nm.[13] In the present range of momentum transfer, flexibility effects have a negligible influence on the single particle form function. The fragment dimensions were estimated from scattering experiments on more diluted isotropic solutions prepared with the same kind of DNA fragments.[38,39] In the liquid crystal, the form function depends on the orientation distribution of the DNA fragments, even in the situation in which the two-dimensional scattering pattern is isotropic. In the parallel configuration, the orientation average of the form function can be accomplished by introducing a Gaussian distribution in tilt angle of individual fragments with respect to the magnetic field. Theoretical form functions have been calculated according to ref 13 with a standard deviation $\sigma = 15°$ and 30° and are displayed in Figure 2. The form function depends moderately on the value of the standard deviation. The values of $\sigma$ are in the range of those estimated from the anisotropic scattering in the $B_\perp$ configuration (see below). The form function corresponding to an isotropic orientation distribution is also included in Figure 2. In 1.5 M NaCl, the maximum intensity agrees reasonably with the value of the form function. For the other samples, substantial differences are observed, irrespective of the chosen distribution width. This is most

noticeable for the simple salt-free solution. These differences show the importance of intermolecular interferences at and beyond the peak maximum for solutions with low ionic strength.

These results can be tentatively explained in terms of an effective DNA radius. As the ionic strength increases, the negatively charged phosphate groups are more effectively screened. In the theory of charged rods an effective diameter is introduced, which decreases with increasing ionic strength.[15-17] Effective diameters have been calculated according to eq 10 and are collected in Table 2 (together with the related values of the twist parameter $h$). The diameters are obtained using a numerical solution of the Poisson–Boltzmann equation for cylindrical polyelectrolytes with excess simple salt. In case of 1–1 simple electrolytes, the results are within 0.6% of those obtained from Philip and Wooding's approximate analytical solution.[40] In solutions without added simple salt, screening is assumed to originate from the uncondensed counterion fraction only. This is a poor approximation, which renders the corresponding values of the effective diameter questionable. For the solution in 0.08 M $MgCl_2$ possible condensation of $Mg^{2+}$ has been neglected. If all $Mg^{2+}$ ions are considered to be condensed, the calculated value of the effective DNA diameter increases by 5%. As shown by Figure 2, with decreasing ionic strength intermolecular interferences become progressively more important. The concurrent increase in effective diameter restricts fluctuations and enhances positional order.

**Anisotropic Scattering Analysis.** In the $B_\perp$ configuration, the scattering pattern is anisotropic. The magnetic field is applied in the direction of the horizontal axis of the detector. Two maxima in intensity are observed at $\alpha = 0°$ and $\alpha = 180°$, $\alpha$ being the angle between the momentum transfer vector and the horizontal axis of the detector. To analyze the anisotropy, the data are rebinned into angular segments of 10°. The results obtained on the four different detector quadrants have been averaged. All intensities have been collected at the same absolute value of momentum transfer $|\mathbf{q}_m| = 1.8\ nm^{-1}$ and are divided by the constant $c\bar{b}_m^2$. The data displayed in Figure 5 refer to the perpendicular configuration with a magnetic field strength of 1.65 T.

As shown by Figure 5, the anisotropy is moderate and decreases with increasing ionic strength (the data are shifted along the $y$-axis to avoid confusing overlap). The ionic strength effect can be interpreted in terms of a change in DNA fragment orientation order. For this purpose, the experimental results are compared to the $\alpha$-dependence of the form function of a uniform rod including a Gaussian distribution of rod orientation with respect to the magnetic field. The solid lines in Figure 5 represent the theoretical results according to eq 6, with the standard deviations $\sigma$ collected in Table 2. The values of $\sigma$ are optimized to the experimental data, with an estimated experimental accuracy of the order of plus or minus 10%. For the sample without added simple salt (sample I), the magnetic field strength dependence of the orientation order has been investigated. Table 2 also includes $\sigma$ of sample I at $B_\perp = 0.8$ and 1.5 T, and previously reported results on samples G1–G3 at a field strength $B_\perp = 0.8$ T. It is clear that $\sigma$ depends on both ionic strength and applied magnetic field strength.

As was demonstrated for the angular averaged intensities in the parallel configuration, high $|\mathbf{q}|$ intermolecular interferences are significant for solutions with low ionic strength. In the anisotropic data analysis, it

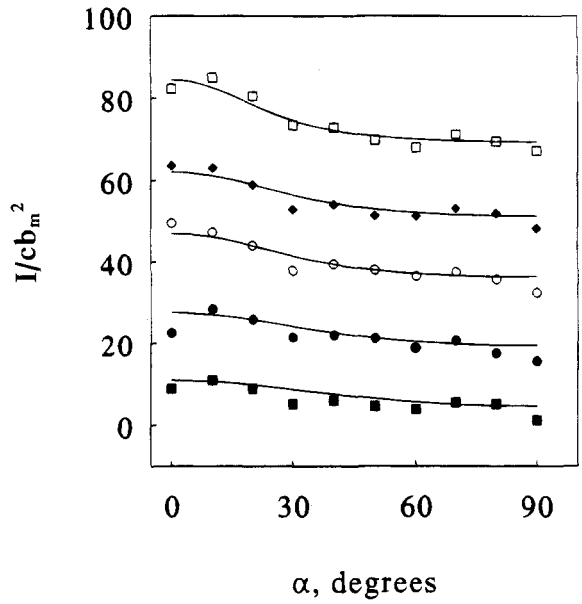


**Figure 5.** The $\alpha$-dependence of the scattering at $|\mathbf{q}_m|$ in the $B_\perp$ configuration. The data points are shifted along the $y$-coordinate to avoid confusing overlap. Sample: (□) I (+60); (◆) II (+45); (○) V (+30); (●) III (+15); (■) IV. The solid lines represent the $\alpha$-dependence of the theoretical form function with $\sigma$ = 15, 20, 20, 25, and 30° from top to bottom.

is assumed that these contributions are $\alpha$-independent and were estimated to be 5.6, 2.6, and 3.2 for samples I, II, and V, respectively. For the high ionic strength samples in 0.75 and 1.5 M NaCl, interference effects at the peak position are negligible. In the perpendicular configuration, the residual interference effects are similar to those in the parallel configuration. The estimated ($\alpha$-independent) intermolecular contributions were added to the theoretically calculated form functions. For solutions with low ionic strength, the derived values of $\sigma$ may differ from the true values if the intermolecular interferences are anisotropic.

The present analysis of the anisotropy differs from the analytic method presented by Deutsch,[41] which is based on an integral equation proposed by Leadbetter and Norris.[42] In this model it is assumed that the molecules are clustered in domains over a distance scale exceeding $1/|\mathbf{q}_m|$, in which the orientations are well correlated. In case of perfect orientation correlation, the interference contribution has the same $\alpha$-dependence as the form function. However, the orientation pair correlation as well as the size of the hypothetical domains cannot be assessed from the data. Furthermore, theoretical work based on the second virial approximation shows a rather wide distribution in fragment orientation (see below). For the lyotropic DNA liquid crystal, the assumption of perfect orientation correlation cannot be maintained and the method due to Leadbetter and Norris is considered to be less suitable.

The value of $\sigma$ refers to a distribution in cholesteric axis orientation and/or a distribution of tilt angle of the individual DNA fragment with respect to the cholesteric axis. The former effect is expected to depend on applied magnetic field strength. In Figure 4 it was already observed that for sample I (without added simple salt) an increase of the magnetic field strength from 0.8 to 1.65 T results in a 15% increase in angular averaged intensity. Indeed, a full two-dimensional analysis shows that $\sigma$ decreases from 20 to 15° when $B_\perp$ increases from 0.8 to 1.65 T. For $B_\perp = 1.5$ and 1.65 T, a small difference in angular averaged intensity is observed (Figure 3).

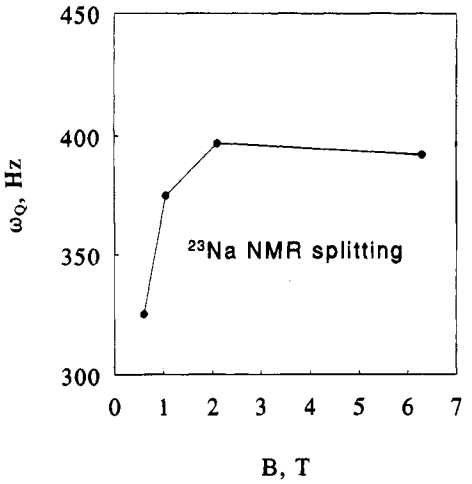


**Figure 6.** Sodium quadrupolar NMR splitting of a 0.44 nucleotide/nm$^3$ NaDNA liquid crystal at 293 K.[44]

This difference is not resolved in the derived value of $\sigma$, due to the poor two-dimensional signal to noise ratio. Furthermore, it should be noted that there is reasonable agreement between the present results and the previously reported value of $\sigma$ under similar experimental conditions (see Table 2, samples G2 and I with $B_\perp$ = 0.8 T).

A magnetic field dependence of the induced alignment is also indicated by the $^{23}$Na NMR quadrupolar splitting. This splitting is displayed in Figure 6 as a function of magnetic field strength.[43,44] In the range 2.1–6.3 T the splitting is approximately constant. For 0.6 and 1.06 T, the splitting decreases about 10 to 5%, respectively. For the higher magnetic field strength, no inhomogeneous broadening of the sodium resonance was observed. This indicates a homogeneity in cholesteric structure with a distribution in cholesteric axis orientation less than 1°. The latter maximum value has been estimated from the NMR experimental accuracy and the orientation order obtained from the present neutron-scattering experiments. With the available magnetic field strengths, full saturation of the angular-averaged neutron-scattering intensity could not be realized. However, in view of the NMR data, a contribution of the distribution in cholesteric axis orientation is probably negligible for $B_\perp$ = 1.65 T. In this situation, the value of $\sigma$ refers exclusively to a distribution of tilt angle of the DNA fragment with respect to the cholesteric axis.

**Comparison with Second Virial Theory.** The ionic strength dependence of the distribution width can be interpreted in terms of the effective DNA excluded volume. Figure 7 displays $\sigma$ versus the product of the DNA fragment concentration $c_p$ (=$c/N_m$, with $N_m$ the number of nucleotides per fragment) and the second virial coefficient $b^{eff}$. The second virial coefficient has been calculated according to eq 9 and the effective diameters collected in Table 2. The new data refer to a similar DNA concentration and a magnetic field strength 1.65 T. Figure 7 includes as well previously reported results on samples G1–G3 at three different DNA concentrations, but without added simple salt. The latter samples were measured with $B_\perp$ = 0.8 T. As was observed for sample I, an increase in magnetic field strength from 0.8 to 1.65 T results in a 5° decrease in distribution width. The samples G1–G3 data displayed in Figure 7 have been corrected accordingly.

The importance of ionic strength for the orientation order is most clearly demonstrated by comparison of the

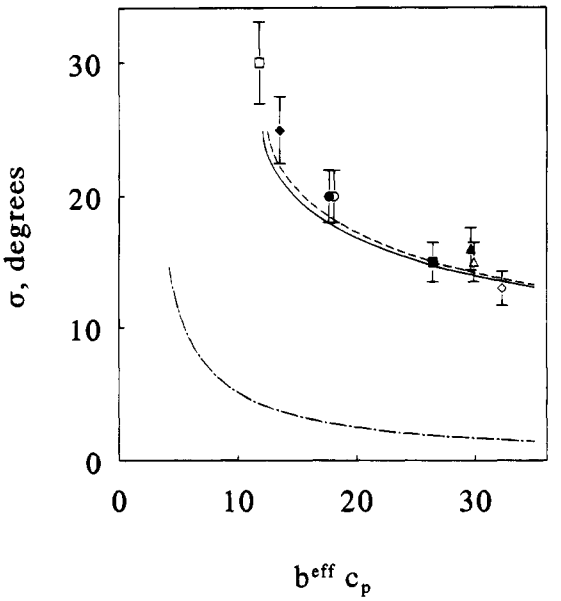


**Figure 7.** Standard deviation $\sigma$ versus the product of the DNA fragment concentration and the second virial coefficient. Symbols from left to right: (□) IV; (◆) III; (●) II; (○) V; (■) G1; (▲) G2; (△) I; (◇) G3. The lines are calculated according to the free energy minimization and are discussed in the text.

samples in 0.25 M NaCl and 0.08 M $MgCl_2$ (samples II and V, respectively). These samples have approximately the same ionic strength; they differ in ionic species. As displayed in Figure 7, within experimental accuracy they exhibit the same orientation order.

The distribution width can be interpreted in terms of a theory for rodlike liquid crystals based on the second virial approximation. This approximation is expected to work well for large aspect ratios $L/D^{eff}$. For the DNA fragments this ratio varies between approximately 8 for simple salt-free samples up to 17 for the solution in 1.5 M NaCl. The Debye–Hückel approximation and the values of the effective diameter are expected to be reasonable for samples with excess simple salt. For samples without added simple salt the values of the effective diameter are questionable. The theory is expected to have some merits for samples with high supporting simple 1–1 electrolyte concentration.

The dotted-dashed and solid lines in Figure 7 display the standard deviation resulting from numerical minimization of the free energy eq 8, together with the orientation entropy of perfectly rigid or semiflexible rods eq 16 and 17, respectively. For the rigid rod orientation entropy, the theoretical values of the standard deviation resulting from the numerical procedure are similar to the analytical approximation eq 18. However, the latter values are much too low in comparison with the experimental data, even for solutions at high ionic strength. When flexibility is included in the orientation entropy, the second virial approximation yields much better agreement.

The orientation entropy of the semiflexible rod and, hence, the standard deviation are sensitive to the number of persistence length units $N_p$. This is especially noticeable when $N_p$ is of order unity. The excluded volume parameters have been calculated with a contour length $L$ = 55 nm. The persistence length $L_p$ is commonly believed to be approximately 50 nm, although for DNA in Θ conditions and/or high salt concentrations lower values of the order 30 nm have been reported.[45–47] In the present dense systems, an ionic strength dependent electrostatic contribution to

the persistence length is negligible.[48,49] The solid line in Figure 7 has been calculated with $N_p = 1.4$ and is in reasonable agreement with the experimental data. This suggests a persistence length $L_p \approx 40$ nm, provided the contour length $L$ equals 55 nm. Another explanation for the relatively large value of $N_p$ is DNA polydispersity. The samples contain an amount of high and low molecular weight DNA material, which might have a serious influence on the phase diagram and distribution width.

The solid and dotted-dashed lines in Figure 7 have been calculated with the twist parameter $h = 0$. The experimental values of $h$ are of the order of 0.1 (see Table 2). The dashed line in Figure 7 refers to the semiflexible case with $h = 0.1$. It is seen that the twist effect on the orientation distribution width is moderate. A similar effect is observed if the approximations of $\varrho$ and $\eta$ (eqs 14 and 15) are carried to higher order (results not shown). The use of effective diameters yields already quite acceptable results.

The sample in excess 1.5 M NaCl (sample IV) is just above the biphasic regime. Further dilution results in phase separation into a coexistent isotropic and anisotropic phase. The boundary concentrations are usually calculated with the help of the coexistence equations.[18] In the semiflexible situation with eq 17, this procedure yields poor results. A small error in the entropy contribution propagates into a serious deviation of the phase diagram.[20] In the calculation of the standard deviation, the free energy can be minimized for $b^{eff}c_p$ exceeding a certain critical value depending on $h$ and $N_p$. For $h = 0$ and $N_p = 1.4$ this critical value amounts to 12.1, which is in reasonable agreement with the corresponding experimental figure 11.8 (sample IV). This supports the use of the persistence length $L_p = 40$ nm. Furthermore, the diverging behavior of $\sigma$ upon approaching the critical value of $b^{eff}c_p$ is theoretically reproduced.

## Conclusions

The characteristic scattering patterns are similar to the results reported before on simple salt-free solutions.[13] The intensities show a single diffraction peak, which owes its existence to intermolecular interferences. The patterns are circular, there is no difference in characteristic intermolecular distance in the direction along and perpendicular to the cholesteric axis. With increasing ionic strength, the peak intensity decreases and, eventually, takes the value of the intraparticle form function. This indicates an increase in position disorder, allowed by a concurrent decrease in effective DNA diameter. A quantitative interpretation of intermolecular interferences is lacking, since this requires a complete description of the orientation and position pair correlation of two highly charged semiflexible rods.

The orientation distribution of the DNA fragments can be inferred from the anisotropic scattering patterns in the perpendicular configuration. For this purpose, the scattered intensities are compared to the form function of a uniform rod, including a Gaussian distribution function. Any possible anisotropy in intermolecular interferences has been neglected. For solutions at low ionic strength, these interferences are most noticeable and the corresponding derived experimental values of $\sigma$ may deviate from the true values. Further work to quantify the importance of these effects in the analysis of anisotropic scattering data is certainly called for.

The distribution width refers to a distribution in cholesteric axis orientation and/or a distribution of tilt angle of an individual DNA fragment with respect to the cholesteric axis. A magnetic field dependence of $\sigma$ has been observed in the range 0.8–1.65 T. Full saturation of the angular averaged intensity was not observed. However, it can be inferred from the NMR data that for 1.65 T the liquid crystal is nearly completely aligned and $\sigma$ refers almost exclusively to a distribution of tilt angle with respect to the cholesteric axis.

The distribution width depends on ionic strength and ranges from 30° in 1.5 M excess simple salt to 15° in simple salt-free solutions. Although at low ionic strength the experimental values of $\sigma$ may be flawed (due to a possible anisotropy in intermolecular interference effects), the data are in quantitative agreement with the second virial theory in the whole ionic strength range. It is necessary to take into account semiflexibility effects in the orientation entropy. The Onsager theory for rigid rods yields too low values of the distribution width. An intrinsic DNA persistence length $L_p \approx 40$ nm is suggested. This figure is somewhat lower than the often quoted value 50 nm. Although for DNA in Θ conditions and/or at high supporting salt concentration values of the order of 30 nm have been reported,[45–47] several alternative explanations can be given. To be mentioned are the neglect of flexibility effects in the excluded volume $[b^{eff}(\varrho + h\eta)]$, DNA polydispersity effects (the material is not completely monodisperse), and neglect of higher virial coefficients. Especially, the latter neglect may be serious for solutions at low ionic strength characterized by a moderate $L/D^{eff}$ aspect ratio.

The effective double layer thickness has been estimated from the Poisson–Boltzmann equation and its ionic strength dependence agrees with the results. It should be stressed that there is no justification of this procedure for solutions without excess simple salt. For the latter solutions, $\sigma$ shows a moderate dependence on $c_p b^{eff}$ and, hence, is rather insensitive to the value of the effective diameter. Furthermore, there is no specific effect of divalent $Mg^{2+}$, the data obtained in $MgCl_2$ are similar to the results in NaCl at approximately the same ionic strength.

**Acknowledgment.** The staff of the ISIS facility is gratefully acknowledged for technical support. We are indebted to the Nederlandse Organisatie voor Wetenschappelijk Onderzoek (NWO) for financial support. G. Jannink, J. C. Leyte, M. Mandel, and Th. Odijk are acknowledged for their contributions in stimulating discussions. Th. Odijk is especially thanked for drawing attention to the importance of semiflexibility effects in the orientation entropy and end effects in the excluded volume parameter. J. A. P. P. van Dijk is acknowledged for performing gel permeation chromatography experiments.

## References and Notes

(1) Reich, Z.; Wachtel, E. J.; Minsky, A. *Science* **1994**, *264*, 1460.
(2) Livolant, F. *Physica A* **1991**, *176*, 117.
(3) Leforestier, A.; Livolant, F. *Biophys. J.* **1993**, *65*, 56.
(4) Robinson, C. *Tetrahedron* **1961**, *13*, 219.
(5) Livolant, F.; Levelut, A. M.; Doucet, J.; Benoit, J. P. *Nature* **1989**, *339*, 724.
(6) Durand, D.; Doucet, J.; Livolant, F. *J. Phys. II Fr.* **1992**, *2*, 1769.
(7) Rill, R. L.; Strzelecka, T. E.; Davidson, M. W.; van Winkle, D. H. *Physica A* **1991**, *176*, 87.
(8) Brandes, R.; Kearns, D. R. *J. Phys. Chem.* **1988**, *92*, 6836.

(9) Maret, G.; Schickfus, M. V.; Mayer, A.; Dransfeld, K. *Phys. Rev. Lett.* **1975**, *35*, 397.
(10) Maret, G.; Dransfeld, K. *Physica B* **1977**, *86–88*, 1077.
(11) Senechal, E.; Maret, G.; Dransfeld, K. *Int. J. Biol. Macromol.* **1980**, *2*, 256.
(12) de Gennes, P. G.; Prost, J. *The Physics of Liquid Crystals*, 2nd ed.; Oxford University Press: Oxford, U.K., 1993; Chapter 6.
(13) Groot, L. C. A.; Kuil, M. E.; Leyte, J. C.; van der Maarel, J. R. C.; Heenan, R. K.; King, S. M.; Jannink, G. *Liq. Cryst.* **1994**, *17*, 263.
(14) Fraden, S.; Maret, G.; Caspar, D. L. D. *Phys. Rev. E* **1993**, *48*, 2816.
(15) Brenner, S.; Parsegian, V. A. *Biophys. J.* **1974**, *14*, 327.
(16) Fixman, M.; Skolnick, J. *Macromolecules* **1978**, *11*, 863.
(17) Stroobants, A.; Lekkerkerker, H. N. W.; Odijk, Th. *Macromolecules* **1986**, *19*, 2232.
(18) Onsager, L. *Ann. N.Y. Acad. Sci.* **1949**, *51*, 627.
(19) Khokhlov, A. R.; Semenov, A. N. *Physica A* **1981**, *108*, 546; *Physica A* **1982**, *112*, 605.
(20) Odijk, Th. *Macromolecules* **1986**, *19*, 2313.
(21) DuPré, D. B.; Yang, S.-j. *J. Chem. Phys.* **1991**, *94*, 7466.
(22) Oldenbourg, R.; Wen, X.; Meyer, R. B.; Caspar, D. L. D. *Phys. Rev. Lett.* **1988**, *61*, 1851.
(23) Fraden, S.; Maret, G.; Caspar, D. L. D.; Meyer, R. B. *Phys. Rev. Lett.* **1989**, *63*, 2068.
(24) Mahler, H. R.; Cordes, E. H. *Biological Chemistry*, 2nd ed.; Harper & Row: New York, 1971; Chapter 5.
(25) Jacrot, B. *Rep. Prog. Phys.* **1976**, *39*, 911.
(26) Odijk, Th. *J. Chem. Phys.* **1990**, *93*, 5172.
(27) Wang, L.; Ferrari, M.; Bloomfield, V. A. *BioTechniques* **1990**, *9*, 24.
(28) Nicolai, T.; van Dijk, L.; van Dijk, J. A. P. P.; Smit, J. A. M. *J. Chromatogr.* **1987**, *389*, 286.
(29) Liebe, D. C.; Stuehr, J. E. *Biopolymers* **1972**, *11*, 167.
(30) Seeger, P. A.; Hjelm, J. R. *J. Appl. Crystallogr.* **1991**, *24*, 467.
(31) Brandes, R.; Kearns, D. R. *Biochemistry* **1986**, *25*, 5890.
(32) Wang, L.; Bloomfield, V. A. *Macromolecules* **1991**, *24*, 5791.
(33) Wissenburg, P.; Odijk, Th.; Cirkel, P.; Mandel, M. *Macromolecules* **1994**, *27*, 306.
(34) Leforestier, A.; Livolant, F. *Liq. Cryst.* **1994**, *17*, 651.
(35) Oosawa, F. *Polyelectrolytes*; Dekker: New York, 1971.
(36) Manning, G. S. *J. Chem. Phys.* **1969**, *51*, 924.
(37) Mandel, M. *Encyclopedia of polymer science and engineering*, 2nd ed.; John Wiley and Sons, Inc.: New York, 1988; Vol. 11, p 739.
(38) van der Maarel, J. R. C.; Groot, L. C. A.; Mandel, M.; Jesse, W.; Jannink, G.; Rodiguez, V. *J. Phys. II Fr.* **1992**, *2*, 109.
(39) Groot, L. C. A.; Kuil, M. E.; Leyte, J. C.; van der Maarel, J. R. C.; Cotton, J. P.; Jannink, G. *J. Phys. Chem.* **1994**, *98*, 10167.
(40) Philip, J. R.; Wooding, R. A. *J. Chem. Phys.* **1970**, *52*, 953.
(41) Deutsch, M. *Phys. Rev. A* **1991**, *44*, 8264.
(42) Leadbetter, A. J.; Norris, E. K. *Mol. Phys.* **1979**, *38*, 669.
(43) Groot, L. C. A.; van der Maarel, J. R. C.; Leyte, J. C. *J. Phys. Chem.* **1994**, *98*, 2699.
(44) Groot, L. C. A. Unpublished results.
(45) Borochov, N.; Eisenberg, H. *Biopolymers* **1984**, *23*, 1757.
(46) Eisenberg, H. *Acc. Chem. Res.* **1987**, *20*, 276.
(47) Borochov, N.; Eisenberg, H.; Kam, Z. *Biopolymers* **1981**, *20*, 231.
(48) Odijk, Th. *J. Polym. Sci., Polym. Phys. Ed.* **1977**, *15*, 477.
(49) Skolnick, J.; Fixman, M. *Macromolecules* **1977**, *10*, 944.

MA946078F